Coherent streamflow variability in Monsoon Asia over the past eight centuries—links to oceanic drivers

Hung T.T. Nguyen[1], Sean W.D. Turner[2], Brendan M. Buckley[3], and Stefano Galelli[1]

[1]Pillar of Engineering Systems and Design, Singapore University of Technology and Design, Singapore
[2]Pacific Northwest National Laboratory, Washington, USA
[3]Lamont-Doherty Earth Observatory, Columbia University, New York, USA

Key Points:

- Climate-informed dynamic streamflow reconstruction is skillful over most of Monsoon Asia
- Spatial coherence of streamflow suggests water management be coordinated between basins
- Mekong and Chao Phraya are most sensitive among rivers to anomalies in sea surface temperature

Corresponding author: Hung Nguyen, `tanthaihung_nguyen@mymail.sutd.edu.sg`

Abstract

The Monsoon Asia region is home to ten of the worlds biggest rivers, supporting the lives of 1.7 billion people who rely on streamflow for water, energy, and food. Yet, a synoptic understanding of multi-centennial streamflow variability for this region is lacking. To fill this gap, we produce the first large scale streamflow reconstruction over Monsoon Asia (48 stations in 16 countries), spanning the past eight centuries. In making this reconstruction, we develop a novel automated, climate-informed, and dynamic reconstruction framework that is skillful for 46/48 stations. We show that streamflow in Monsoon Asia is spatially coherent, owing to common drivers from the Pacific, Indian, and Atlantic Oceans. We also show that these drivers exert their greatest influence over the Mekong and Chao Phraya basins. We suggest that future water management in the region should be coordinated between basins, taking into account the states of the oceans.

Plain Language Summary

Ten of the world's biggest rivers are located entirely within the Asian Monsoon region. They provide water, energy, and food for 1.7 billion people. To manage these critical resources, we need a better understanding of river discharge—how does it change over a long time? Are there common variation patterns among rivers? To answer these questions, we use information derived from tree rings to reconstruct river discharge history at 48 gauges in 16 Asian countries. Our reconstruction reveals the riparian footprint of megadroughts and large volcanic eruptions over the past eight centuries. We show that simultaneous droughts and pluvials have often occurred at adjacent river basins in the past, because Asian rivers share common influences from the Pacific, Indian, and Atlantic Oceans. We also show that the oceans exert their greatest influences on the Mekong and Chao Phraya basins. From these findings, we suggest that future water management in the region should be coordinated between basins, taking into account the states of the oceans. Our findings can benefit the riparian people of the Asian Monsoon region.

1 Introduction

Of the world's 30 biggest rivers, ten are located within Monsoon Asia, and two others originate from this region (Figure 1). These river basins are home to 1.7 billion people (Best, 2019). With high population densities, even smaller basins support the livelihood of millions—e.g., Chao Phraya (Thailand): 25 million, Angat (the Philippines): 13 million, and Citarum (Indonesia): 10 million (Nguyen & Galelli, 2018; Libisch-Lehner et al., 2019; D'Arrigo et al., 2011). River discharge, or *streamflow*, provides water for domestic and industrial uses, irrigation, and hydropower. It sustains aquatic life (including fish yield), carries sediment and nutrients, and enables navigation. Streamflow is an important link in both the water-energy-food nexus and the ecological cycle. To manage this resource, we need a good understanding of hydrologic variability. Such understanding is often derived from streamflow measurements; however, these instrumental data span typically only a few decades, too short to capture long-term variability and changes in streamflow.

When compared against instrumental data, longer streamflow records reconstructed from climate proxies—such as tree rings—often reveal striking insights. A reconstructed pre-dam variability of the Yellow River (Li et al., 2019) shows that streamflow in 1968–2010 was only half of what should have been; in other words, human activities depleted half of the available water! A reconstruction of the Citarum River (Indonesia) (D'Arrigo et al., 2011) shows that the period 1963–2006 contained an increasing trend of low flow years but no trend in high flow years, compared with the previous three centuries. This finding suggests that 10 million inhabitants of Jakarta may be facing higher drought risks than what is perceived from the instrumental record. The Mongolian "Breadbasket", an agricultural region in north-central Mongolia (Pederson et al., 2013), experienced an unusually wet twentieth-century, and the recent dry epoch is not rare in the last four centuries (Davi et al., 2006; Pederson et al., 2013; Davi et al., 2013). Consequently, agricultural planning cannot take the twentieth century to be the norm, lest history repeats the lesson of the Colorado River Basin: observations over abnormally wet years (Stockton & Jacoby, 1976; Woodhouse et al., 2006; Robeson et al., 2020) led to water rights overallocation, and the Colorado no longer reaches the Pacific Ocean.

Compelling evidence calls for more streamflow reconstructions in Monsoon Asia. Tremendous efforts, booming in the last four years (Figure S1), have partly addressed this need, but the hydrological knowledge gained was limited to individual catchments, more than half of which are in China (Figure S1 and Table S1). A synoptic understanding is lacking. Here, we produce the first large scale streamflow reconstruction for Monsoon Asia, covering 48 stations in 16 countries, unraveling eight centuries of annual streamflow variability. To achieve this task, we develop a novel automated framework with three main components: (1) a climate-informed proxy selection procedure, (2) a dynamic state-space reconstruction model, and (3) a rigorous cross-validation routine for parameter tuning to achieve optimal skills. We also use the Monsoon Asia Drought Atlas version 2 as the paleoclimate proxy instead of a tree ring network, as the former offers computational advantages (supported with strong physical and statistical foundations) for this large scale reconstruction. With this work, 44 stations are reconstructed for the first time while the other four (Citarum, Yeruu, Ping, and Indus Rivers) are extended back in time compared to previous works (D'Arrigo et al., 2011; Pederson et al., 2013; Nguyen & Galelli, 2018; Rao et al., 2018). This data set allows us to assess both local historical water availability and regional streamflow patterns, revealing the spatial coherence of streamflow and its links to the oceans. This understanding may improve interbasin water resources management and coordination.

2 Data

2.1 Streamflow Data

We obtained streamflow data from the Global Streamflow Indices and Metadata Archive (GSIM) (Do et al., 2018; Gudmundsson et al., 2018), using stations having at least 41 years of data, with less than 3% missing daily values, and with mean annual flow of at least 50 m^3/s. We also received streamflow data from our colleagues for some countries where public streamflow records are not available (see Acknowledgment).

Many stations in our collection have upstream reservoirs that may interfere with the proxy-streamflow relationship. This interference is stronger for seasonal streamflow than annual streamflow: reservoirs transfer water from the wet season to the dry season, but not all reservoirs retain water from year to year. Reservoirs that are filled and emptied within a year do not change the annual water budget downstream. To minimize reservoir interference, we reconstructed annual streamflow, and we removed stations that have upstream retention time longer than a year. We identified upstream reservoirs by overlaying the Global Reservoirs and Dams (GRanD) data (Lehner et al., 2011) on the river network (Lehner & Grill, 2013; Barbarossa et al., 2018). The upstream retention time was calculated as the total upstream reservoir capacity (million m^3) divided by the mean annual flow volume (million m^3/year). For stations having over-year reservoirs constructed towards the end of their records, we also truncated the corresponding years, keeping only the streamflow data before dam construction.

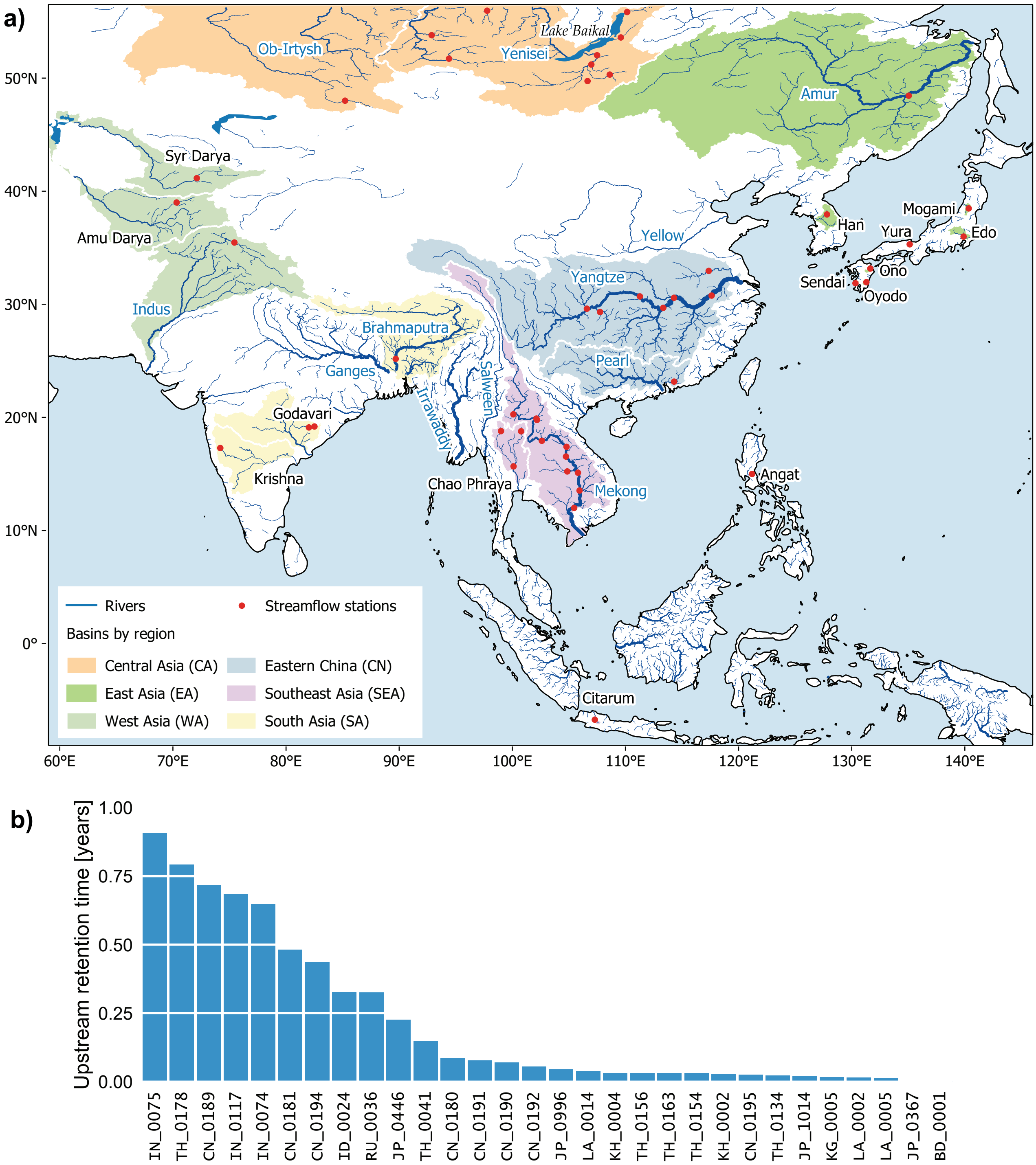

Figure 1. Study region. a) The Monsoon Asia region (Cook et al., 2010); river basins involved in this study are highlighted by sub-region, rivers belonging to the world's 30 biggest (Best, 2019) shown with blue names. b) Upstream retention time of the 30 stations that have upstream reservoirs. Refer to Table S2 for station details.

Our collection and quality control effort resulted in an annual streamflow data set of 48 stations in 16 countries. We used the calendar year (January to December) as there is not a common water year across the study domain (Knoben et al., 2018). The stations' locations and upstream retention times (for those having upstream reservoirs) are shown in Figure 1. More metadata are supplied in Table S2.

2.2 Proxy Data

Our paleoclimate proxy is the Monsoon Asia Drought Atlas version 2 (MADA v2) (Cook, 2015), built upon the original MADA of Cook et al. (2010). The MADA is a gridded data set of the Palmer Drought Severity Index (PDSI) (Palmer, 1965) over the Asian monsoon region; each grid cell contains an annual time series of the mean June-July-August PDSI, reconstructed from tree rings, and calibrated with the instrumental data set of Dai et al. (2004). The MADA proves to be a reliable long-term record of monsoon strength, having revealed the spatiotemporal extents of the four Asian megadroughts in the last millennium, and linking variations in monsoon strength to sea surface temperature patterns. MADA v2 improves over its predecessor by incorporating more tree ring chronologies (453 versus 327), and targeting the self-calibrating PDSI (scPDSI), which addresses several limitations of the standard PDSI (Wells et al., 2004; van der Schrier et al., 2013). We use the MADA v2 portion between 1200–2012 as this is the common period of most grid points in the atlas (Figure S4), and is also the stable portion with sufficient sample depth in the source tree ring network.

Drought atlases (reconstructed from tree rings) have been shown to be good paleoclimate proxies for streamflow reconstruction: since both streamflow and PDSI can be modeled as functions of ring width, one can also build a model to relate streamflow to PDSI (Ho et al., 2016, 2017; Nguyen & Galelli, 2018). Drought atlases enhance the spatial expression of the underlying tree ring data—by incorporating the modern PDSI field in its calibration—and are also more uniform in space and time than the tree ring network itself (see Cook et al., 2010, Figure 1), making them better suited to large scale studies. We now elaborate these points as we describe the methodology.

3 Methods

3.1 Using a Drought Atlas as Paleoclimate Proxy

3.1.1 Physical basis

The main physical processes that involve climate and tree growth are depicted in Figure 2a. The climate at a given location can be characterized by precipitation and temperature, among others. These climatic inputs control soil moisture on land. Except for losses (such as groundwater recharge, evaporation, and surface runoff), the net soil moisture storage then follows two main paths: one goes out of the catchment as streamflow, the other is taken up by the trees and transpired back into the atmosphere, influencing tree growth along the way. Thus, tree growth and streamflow are connected via land-atmosphere interactions—this is the basis for streamflow reconstruction from tree ring. Note, however, that tree growth does not directly control streamflow, and neither does streamflow control tree growth; we can infer a relationship between them only because they are both influenced by soil moisture. On the other hand, soil moisture directly controls streamflow and is, in principle, a reasonable predictor for streamflow.

It would thus be ideal to have a "natural" soil moisture proxy record, but of course that is not the case. We can instead rely on a surrogate—a soil moisture record reconstructed from tree rings, such as the MADA.

3.1.2 Statistical basis

The physical discussion above yields three types of paleoclimate reconstruction: streamflow from tree rings, soil moisture from streamflow, and streamflow from soil moisture. We now derive mathematically the relationships between these reconstruction types.

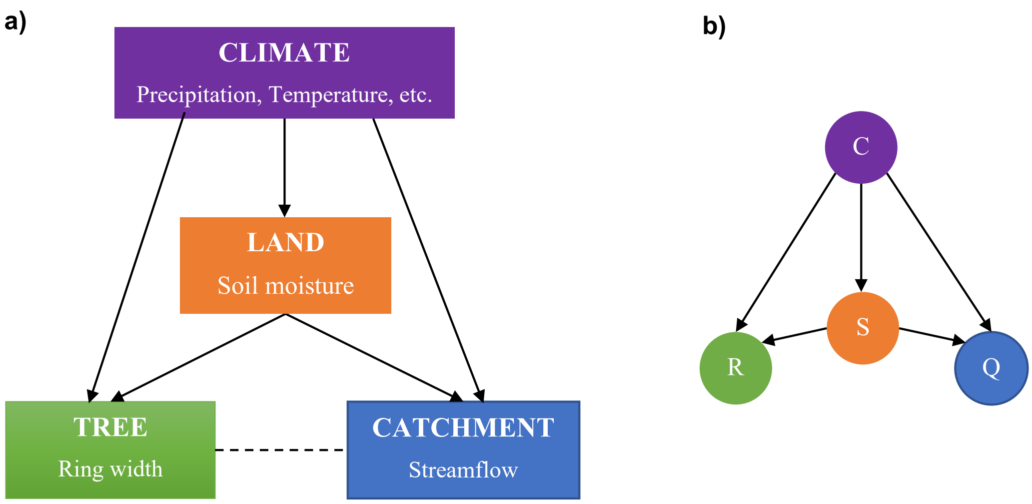

Figure 2. a) Relationships between hydroclimatic variables and tree growth. b) A probabilistic graphical model representing the relationships in a), where C is a vector of climate variables, S the soil moisture, R the ring width index, and Q streamflow. The arrows represent the conditional dependence among variables.

Each reconstruction is a conditional distribution of one variable (e.g. streamflow) given that we have observed another variable (e.g. soil moisture), and given the historical climate. We represent these conditional distributions with a probabilistic graphical model (Koller & Friedman, 2009) as shown in Figure 2b. There are four random variables involved: climate (C), soil moisture (S), ring width (R), and streamflow (Q). Each of these variables can be multivariate, i.e., C includes precipitation and temperature, among others, and all variables can include multiple sites or grid points. As a convention, let $f_X(x)$ be the probability density function (PDF) of the random variable X, $f_{XY}(x, y)$ be the joint PDF of X and Y, and $f_{X|Y}(x|y)$ be the conditional PDF of X given that $Y = y$.

Reconstructing streamflow from tree ring is essentially deriving the distribution of Q given R and C, i.e, $f_{Q|R,C}(q|r, c)$, where r is the measured ring width index, and c is the historical climate. We can decompose this distribution as follows:

$$\begin{aligned} f_{Q|R,C}(q|r,c) &= \int f_{Q,S|R,C}(q,s|r,c)\,ds \\ &= \int f_{Q|S,R,C}(q|s,r,c) f_{S|R,C}(s|r,c)\,ds. \end{aligned} \tag{1}$$

The first equality comes from the relationship between marginal and joint distributions. The second equality comes from Bayes' theorem. Now, Q is independent of R given S and C (Figure 2b), so $f_{Q|S,R,C}(q|s, r, c) = f_{Q|S,C}(q|s, c)$. Consequently,

$$f_{Q|R,C}(q|r,c) = \int f_{Q|S,C}(q|s,c) f_{S|R,C}(s|r,c)\,ds. \tag{2}$$

Observe that $f_{Q|S,C}$ is the streamflow reconstruction from the MADA, and $f_{S|R,C}$ is the MADA reconstruction from tree rings. Thus we have established mathematically the reasoning that tree-ring-based streamflow reconstruction is possible based on the link through soil moisture. $f_{Q|R,C}$ is the marginal distribution without observing the soil moisture. Instead of constructing $f_{Q|R,C}$, we can infer S from R, then Q from S, by constructing $f_{S|R,C}$ and $f_{Q|S,C}$.

3.1.3 Computational advantages of using the MADA, and a caveat

The MADA can be thought of as a transformation from the tree ring network, irregular in both space and time, to a regular grid with homogeneous temporal coverage—analogous to transforming meteorological station data to gridded temperature and precipitation products. This transformation brings several advantages to reconstructing streamflow using the MADA, compared to using the underlying tree ring network.

First, in a typical reconstruction study, one must detrend and standardize the tree ring data to remove non-climate signals (cf. Cook and Kairiukstis (1990)). For a large scale study like ours, such a task is complex. Instead, we can leverage the effort that has been devoted to detrending and standardizing the chronologies in making the MADA, and use the MADA as proxy, having built the physical and statistical foundations to do so.

Second, the tree ring sites often cluster, with vast empty space between clusters (see e.g. Cook et al. (2010), Figure 1). When taking a subset of them for reconstruction at a station, there can be cases where none or very few sites are within a search radius. The MADA helps "bridging" the space, bringing climate signals from further-away tree sites to grid points nearer to the station. The high resolution grid ($1^\circ \times 1^\circ$ for version 2) makes automated grid point selection easier. (The automated grid point selection procedure is described in Section 3.2.1.)

Third, when reconstructing streamflow from tree rings, nested models are often necessary because tree ring chronologies have different time spans. One starts with the shortest nest, using the common time span of all chronologies to build a model, then dropping the shortest chronology to build a second model with longer time span but less explained variance than the first, and repeating the process, dropping more chronologies to achieve longer time spans until the final nest with the longest time span, but with the lowest explained variance. The nests' outputs are then corrected for their variance and averaged to obtain the final reconstruction (see e.g. D'Arrigo et al. (2011)). This nesting step was carried out for the MADA, such that most grid points have the same time span (Figure S4). This lets us use a single common period (1200-2012), and eliminates our need to build nested models back in time. This is particularly desirable for our dynamic state-space reconstruction model, as averaging the nests breaks the link between the catchment state and streamflow. (The reconstruction model is described in Section 3.2.2).

The computational advantages of using the MADA are thus threefold: (1) no detrending and standardization, (2) easier grid point selection, and (3) no nesting. However, these come with a cost: uncertainty. When reconstructing streamflow from the MADA, we treat the MADA (i.e, the model input) as constant. But in fact, the MADA is a regression product and has its own uncertainty. Incorporating this uncertainty is difficult and is out of the scope of this paper, but it is an interesting topic for further research.

3.2 Climate-informed Dynamic Streamflow Reconstruction

When reconstructing a climate field, such as a PDSI grid or a streamflow station network, it is desirable to preserve the field covariance structure. However, building a large-scale spatial regression model is challenging. Instead, one can reconstruct each point in the field independently, and rely on the proxy network to capture the spatial patterns. This is the premise of the Point-by-Point Regression (PPR) method (Cook et al., 1999), and this principle has led to the successful reconstruction of many drought atlases (Cook et al., 1999, 2010, 2015). Our reconstruction framework is inspired by PPR—we reconstruct station by station—but diverges in several ways. The two key differences are, first, in the way proxy points are selected, and second, in the regression model.

3.2.1 Climate-informed Input Selection

The PPR procedure selects proxy points (tree ring chronologies) within a search radius. Given that geographical proximity does not imply hydroclimatic similarity, we selected our proxies (MADA grid points) by hydroclimatic similarity directly. The hydroclimate at location i (a MADA grid point or a streamflow station) is characterized by three indices: aridity a_i, moisture seasonality s_i, and snow fraction f_i, following Knoben et al. (2018) (hereafter referred to as the KWF system, after the three authors). The hydroclimatic similarity between two locations i and j is then defined as their Euclidean distance in the hydroclimate space. This distance is termed the KWF distance and its mathematical definition is

$$d_{KWF}(i,j) = \sqrt{(a_i - a_j)^2 + (s_i - s_j)^2 + (f_i - f_j)^2}. \tag{3}$$

The KWF distance lets us screen out MADA grid points that are geographically close to the station of interest but hydroclimatically different—a climate-informed grid point selection scheme. Whereas previous PPR implementations varied the search radius, we fixed the radius to 2,500 km—the scale of regional weather systems (Boers et al., 2019)—and varied the KWF distance between 0.1 and 0.3 in 0.05 increments. For reference, the maximum KWF distance between any two points in Monsoon Asia is 1.424. Each KWF distance yielded a search region encompassing a set of MADA grid points surrounding the streamflow station of interest. In our search regions, PDSI often correlates significantly and positively with streamflow (Figure 3); indeed hydroclimatic similarity is a physical basis for correlation.

Next, we performed weighted principal component analysis (PCA) to remove multicollinearity among the MADA grid points. Following PPR, we weighted each grid point by its correlation with the target streamflow, using equation (4):

$$z_i = x_i \rho_i^p. \tag{4}$$

Here, x_i is the scPDSI time series at grid point i, ρ_i the correlation between x_i and the target streamflow, p the weight exponent, and z_i the weighted version of x_i. We used

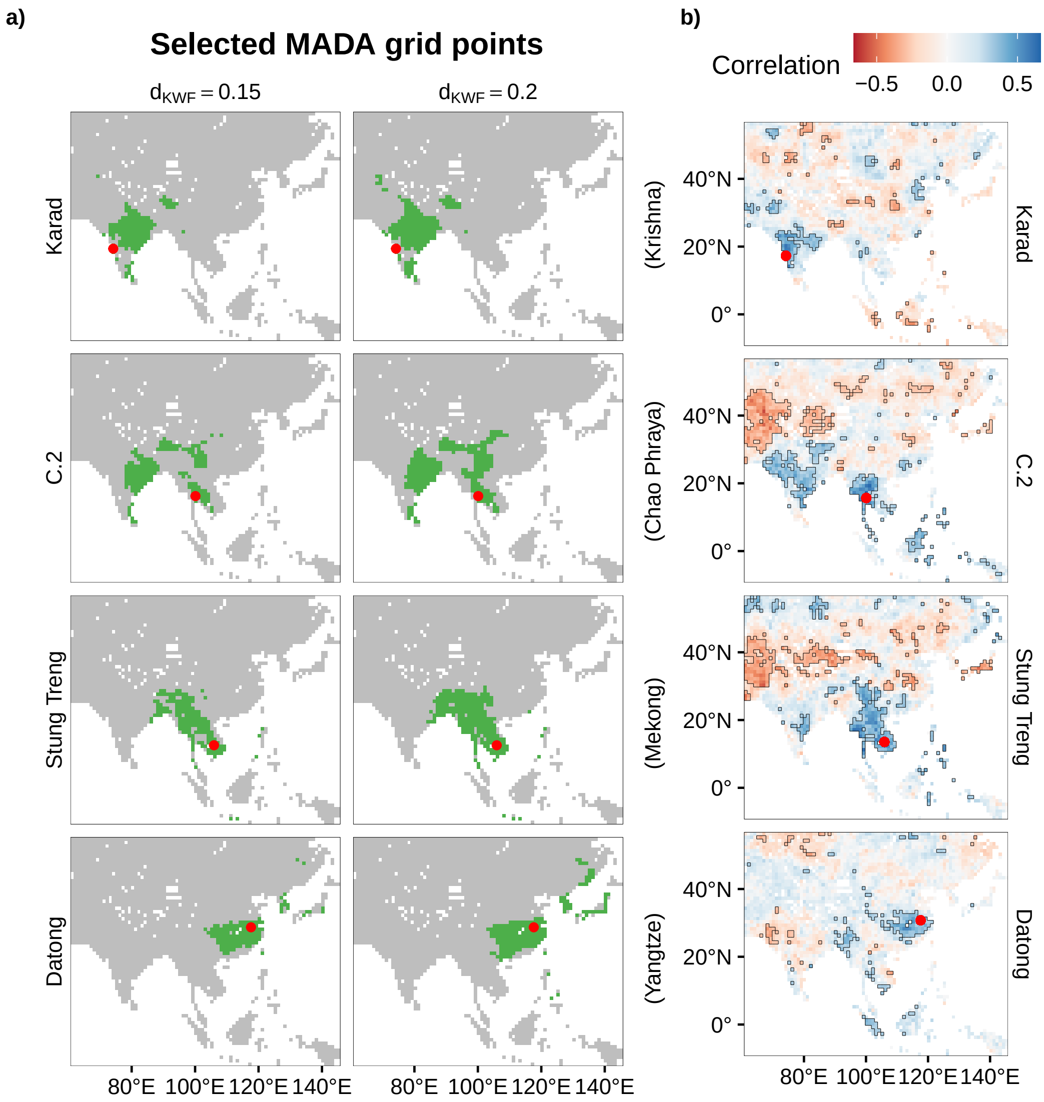

Figure 3. a) Examples of the climate-informed grid point selection: selected MADA grid points (green) based on two KWF distances (columns) at four stations (rows). b) Correlations between streamflow at the same four stations and the MADA, significant correlations ($\alpha = 0.05$) enclosed in black boundaries. The selection regions in (a) generally have significant positive correlation with streamflow. The areas with significant negative correlations need further investigation.

$p = 0, 0.5, 2/3, 1, 1.5,$ and 2, the same as those used by Cook et al. (2010). We then performed PCA on z_i's, and retained only those principal components having eigenvalue at least 1.0 (Hidalgo et al., 2000). We further reduced this subset using the VSURF (Variable Selection Using Random Forest) algorithm (Genuer et al., 2010). So, for each combination of KWF distance and PCA weight, we arrived at a subset of principal components for reconstruction. Each streamflow station has an ensemble of 30 such subsets, the best of which was identified using cross-validation (Section 3.2.3) and used for the final reconstruction.

3.2.2 Linear Dynamical System

Having obtained the climatic inputs, the next step was to model the relationship between these inputs and the catchment output (streamflow). Here, this relationship was not modeled with linear regression (as with original PPR, and as typical with previous reconstruction studies), but as a linear dynamical system (LDS), following equations (5) and (6):

$$x_{t+1} = Ax_t + Bu_t + w_t \tag{5}$$

$$y_t = Cx_t + Du_t + v_t \tag{6}$$

where t is the time step (year), y the catchment output (streamflow), u the climatic input (an ensemble member from the climate-informed grid point selection), w and v white noise, and x the system state, which can be interpreted as the catchment's flow regime, i.e, wet or dry (Nguyen & Galelli, 2018). By modeling the flow regime and its transition, the LDS model accounts for both regime shifts (Turner & Galelli, 2016) and catchment memory (Pelletier & Turcotte, 1997). These behaviors are not modeled in linear regression.

The LDS model assumes that the initial state and the noise processes are normally distributed:

$$w_t \sim \mathcal{N}(0, Q) \tag{7}$$

$$v_t \sim \mathcal{N}(0, R) \tag{8}$$

$$x_1 \sim \mathcal{N}(\mu_1, V_1). \tag{9}$$

It follows that the catchment state and output must also be normally distributed. But some of our streamflow records are skewed. These were log-transformed to reduce skewness (Text S2 and Figure S3).

The LDS model is trained using a variant of the Expectation-Maximization algorithm. In the E-step, we fix the model parameters and learn the hidden state. In the M-step, we fix the hidden state and learn the model parameters. Iterations are repeated between the E- and M-steps until convergence. The reconstruction algorithm is implemented in the R package *ldsr* (Nguyen, 2020a).

3.2.3 Cross-validation

Consistent with the literature, we assessed reconstruction performance using the metrics Reduction of Error (RE) and Nash-Sutcliffe Coefficient of Efficiency (CE or NSE) (Nash & Sutcliffe, 1970; Fritts, 1976). Mathematically,

$$RE = 1 - \frac{\sum_{t\in\mathcal{V}}(Q_t - \hat{Q}_t)^2}{\sum_{t\in\mathcal{V}}(Q_t - \bar{Q}_c)^2} \tag{10}$$

$$CE = 1 - \frac{\sum_{t\in\mathcal{V}}(Q_t - \hat{Q}_t)^2}{\sum_{t\in\mathcal{V}}(Q_t - \bar{Q}_v)^2} \tag{11}$$

where t is the time step, $\mathcal{V}$ the validation set, Q the observed streamflow, $\hat{Q}$ the reconstructed streamflow, $\bar{Q}_c$ the calibration period mean, and $\bar{Q}_v$ the verification period mean. Both RE and CE are based on squared error; they can be sensitive to outliers, especially the CE. To address this limitation, Gupta et al. (2009) proposed another metric, which assesses a model output based on its correlation with observation, as well as its bias and variability (equation (12)):

$$KGE = 1 - \sqrt{(\rho-1)^2 + \left(\frac{\hat{\mu}}{\mu} - 1\right)^2 + \left(\frac{\hat{\sigma}}{\sigma} - 1\right)^2}. \tag{12}$$

Here, ρ is the correlation between model output and observation, $\hat{\mu}$ and μ the modeled and observed mean of the streamflow time series, and $\hat{\sigma}$ and σ the modeled and observed standard deviation of the streamflow time series. This metric is now known as the Kling-Gupta Efficiency (KGE). Compared to the CE, the KGE is more robust to outliers, hence we chose the KGE as the criterion for model selection.

Conventionally, reconstruction skills are often calculated in a split-sample (i.e., two-fold) cross-validation scheme: the model is calibrated with the first half of the data and validated with the second half, then calibrated with the second half and validated with the first half (see e.g. D'Arrigo et al. (2011)). The contiguous halves aim to test a model's ability to capture a regime shift (Briffa et al., 1988). Unfortunately, this scheme is not practical for many stations in our record, where it would leave us only 20–25 data points for calibration (Figure S2). In addition, a two-fold cross-validation scheme provides only two point estimates for each skill score, and they may be notably different (for example, D'Arrigo et al. (2011) reported CE values of 0.21 and 0.73 for the two folds.) As a result, the mean skill score may not be robust. A number of recent works have instead used the leave-k-out cross-validation scheme (e.g. Ho et al. (2016); Li et al. (2019); Chen, Shang, Panyushkina, Meko, Li, et al. (2019)). In this scheme, a random chunk of k data points is withheld for validation while the model is calibrated with the remaining data points, then calibration and validation are repeated over as many as 100 chunks of k. This scheme provides a more robust estimate of the mean skill score, but it may not correctly assess the model's ability to capture a regime shift, because the withheld points are not contiguous like in the split-sample scheme.

We sought a balanced approach. In each cross-validation run for each station, we withheld a *contiguous* chunk of 25% of the data points for validation and trained the model on the remaining 75%. This way, we maintain the goal of the split-sample scheme while still having enough data for calibration and getting a reasonably robust mean skill estimate. We could not get as many contiguous chunks as if they were random, so we repeated the procedure 30 times instead of 100, and calculated the mean KGE over these 30 runs. The ensemble member (cf. Section 3.2.1) that resulted in the highest mean KGE across the 30 cross-validation runs was used for the final reconstruction of each station. The cross-validation procedure is also available in the *ldsr* package.

4 Results and Discussion

4.1 Reconstruction Skills

Reduction of Error (RE) is positive at all stations (Figure 4a and b); Coefficient of Efficiency (CE) is positive at all but two: Nowrangpur (India) on the Godavari, and Ubon (Thailand) on the Nam Mun, a tributary of the Mekong (Figure 4c and d). Both negative values are larger than -0.08. The tree ring network used to build the MADA has lower density in India (Cook, 2015) so CE values here are understandably lower. Ubon, on the other hand, is located in an area of high quality tree ring chronologies (Buckley et al., 2007; Sano et al., 2009; Buckley et al., 2010), yet its variability is not captured by the MADA as well as nearby stations. We suspect there are data errors at this gauge. The histogram of CE resembles that of RE but shifts slightly left—this is expected as CE is a more stringent metric than RE (Cook & Kairiukstis, 1990). Much lower CE than RE implies overfitting; we do not observe that here.

The Kling-Gupta Efficiency (KGE) is all positive, and its histogram leans toward the higher end (Figure 4e and f). It should be noted that if one wishes to benchmark a model against the verification period mean (as is with the CE), the threshold value is $1-\sqrt{2}$, i.e, $KGE > 1-\sqrt{2}$ is analogous to $CE > 0$ (Knoben et al., 2019). The KGE scores in Figure 4 suggest that our reconstruction model performs well in terms of key characteristics: correlation, bias, and variability.

All three metrics have similar spatial distributions (Figure 4a, c, and e). As expected, lower (but positive) skills are seen in most of Central and West Asia, which lie outside

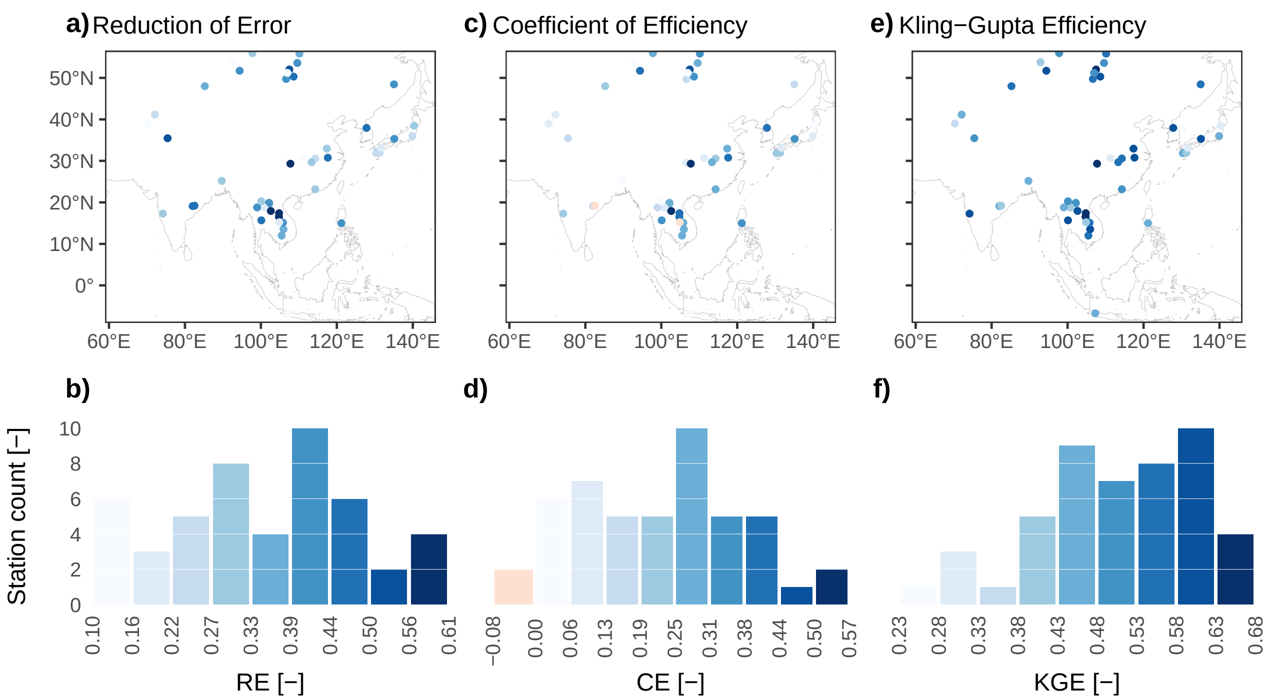

Figure 4. Distribution of model performance scores. Panels a, c, and e show the scores of each station following the color legends encoded with the histograms in panels b, d, and f.

the active monsoon area. An exception is the upper reach of the Selenge River (Mongolia), upstream of Lake Baikal, where model skill is high, owing to high quality tree ring records from Mongolia (Davi et al., 2006; Pederson et al., 2013; Davi et al., 2013; Pederson et al., 2014). In Japan, where the small catchments are sensitive to local climate, model skill is reduced. In all other regions, model skill is homogeneous. The consistent performance of our model suggests that the MADA is a good proxy for streamflow reconstruction in Asia, and our climate-informed dynamic reconstruction is skillful.

As an additional validation exercise, we compared the spatiotemporal variability of reconstructed streamflow against instrumental data for the period 1950–2012 (Figure S5). Our reconstruction captures well the spatial variation patterns of streamflow in this period, as well as the timing, duration, and magnitude of extreme droughts and pluvials.

4.2 Spatiotemporal Variability of Monsoon Asia's Streamflow

Having obtained good skill scores, we now present eight centuries of spatiotemporal streamflow variability in Monsoon Asia (Figure 5). This reconstructed history captures the riparian footprint of major historical events (large volcanic eruptions, megadroughts, and pluvials). We first discuss the impact of the three largest eruptions of the past eight centuries (Sigl et al., 2015): Samalas (1257) (Lavigne et al., 2013), Kuwae (1452-53) (Gao et al., 2006), and Tambora (1815) (Stothers, 1984).

Assuming that Kuwae erupted in 1452 (consistent with tree ring records, see e.g. Briffa et al., 1998), these three eruptions saw a persistent streamflow pattern across Southeast Asia, eastern China, and West Asia. In the eruption year t ($t = 1257, 1452, 1815$), abnormally high streamflow occurred in all three regions. In year t+1, streamflow remained high in Southeast Asia but abruptly turned low in West Asia and parts of eastern China. This is unexpected given the results of Li et al. (2013). They found that in year t, PDSI (captured by the MADA) was negative in all three regions; in year t+1, PDSI remained negative in Southeast Asia but turned positive in West Asia and eastern China. Based on their findings, one would expect streamflow to be low in all three regions in year t, then remain low in Southeast Asia but turn high in West Asia and eastern China in year t+1. We observe the opposite. Interestingly, Anchukaitis et al. (2010), also using PDSI, found in year t wet conditions in Southeast Asia (similar to our results) but mixed wet and dry conditions in eastern China and West Asia (more similar to Li et al., 2013). The disparity in these studies are attributed to the different sets of eruptions used—Anchukaitis et al. (2010) demonstrated this with three sets of events. Our divergence from their results are partly because they used Superposed Epoch Analysis while we analyze individual events, but we argue that the main cause is streamflow versus PDSI. With our streamflow results, we offer a reconciling explanation: during and immediately after the eruptions, PDSI was more driven by temperature than precipitation, and while low temperature may have caused negative PDSI, it reduced evaporation and consequently, increased streamflow. This mechanism is particularly relevant in midlatitude eastern China and West Asia. In Southeast Asia, however, reduced temperature, from warm to cool, could increase soil moisture (Anchukaitis et al., 2010), resulting in high streamflow. Not disagreeing with previous works, our results offer a look at another aspect of past climate using streamflow instead of PDSI.

As a drought/pluvial indicator, streamflow may differ from PDSI in individual years, as discussed above, but on longer terms, our reconstructed streamflow agrees well with reconstructed PDSI. For example, our record fully captures the Angkor Droughts (1345–1374 and 1401–1425) (Buckley et al., 2010, 2014) with prolonged low flow throughout the Mekong and Chao Phraya basins (Southeast Asia). Heavy monsoon rain interrupted these megadroughts; such abrupt alterations to the flow regime proved difficult for Angkor's water managers (Buckley et al., 2014). After the first Angkor Drought, they altered the

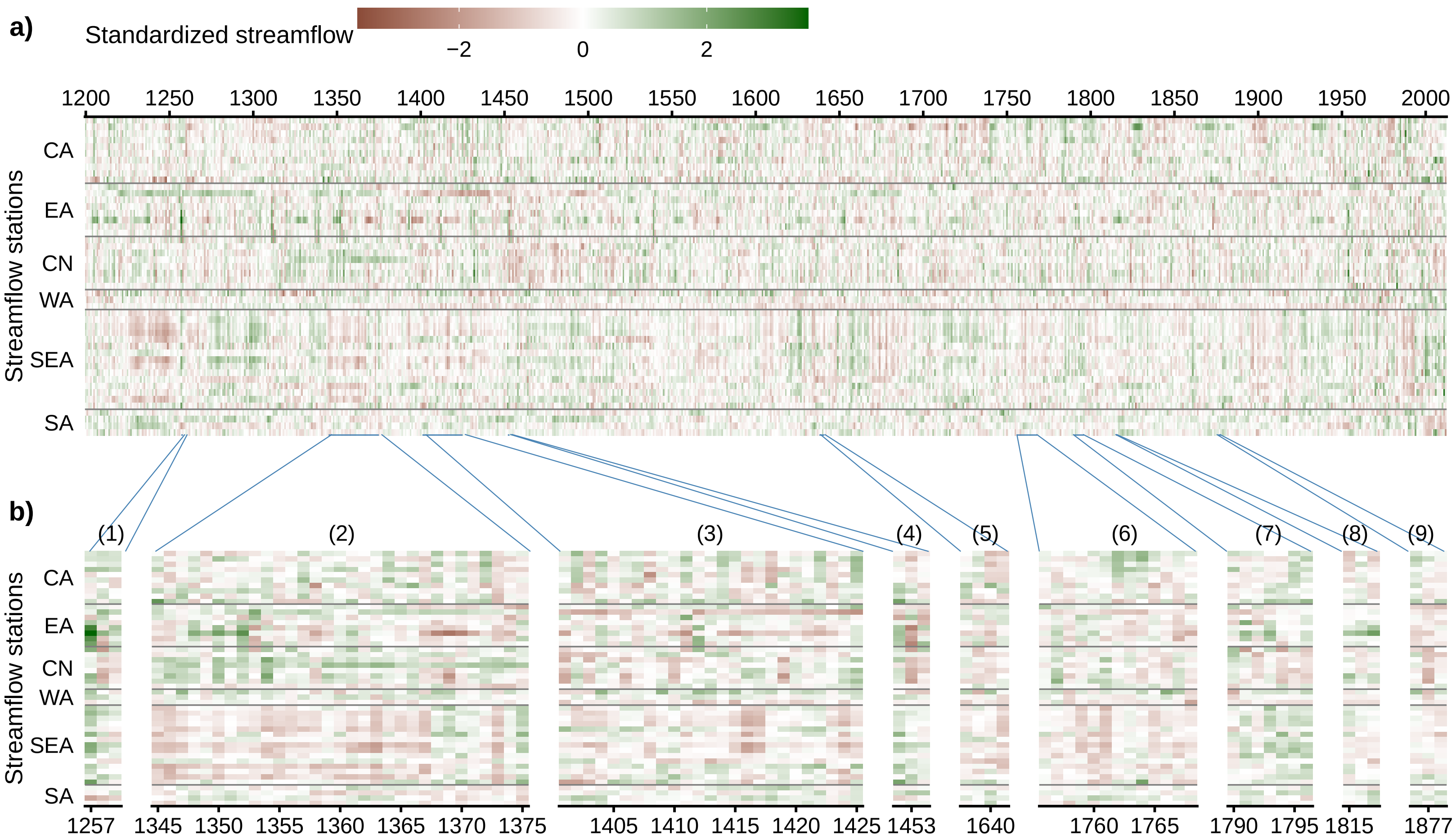

Figure 5. Spatiotemporal variability of streamflow in Asia. a) Variations over time (x-axis) and space (y-axis) of the standardized streamflow index (i.e., z-score of streamflow, or z-score of log-transformed streamflow when log-transformation was used in the reconstruction). The stations are arranged approximately north to south (top down on y-axis) and divided into five regions as delineated in Figure 1: CA (Central Asia), EA (East Asia), WA (West Asia), CN (eastern China), SEA (Southeast Asia), and SA (South Asia). b) Historic events captured in the reconstruction: (1) Samalas eruption, (2) and (3) Angkor Droughts I and II, (4) Kuwae eruption, (5) Ming Dynasty Drought, (6) Strange Parallels Drought, (7) East India Drought, (8) Tambora eruption, and (9) Victorian Great Drought.

inflow/outflow functions of their *barays* (reservoirs) in an attempt to preserve water. Heavy rains and flooding subsequently destroyed the reduced-capacity hydraulic infrastructure. This flood likely occurred in 1375 (Figure 5b, event 2).

By the second Angkor Drought, the hydraulic city had insufficient water storage and could not recover. Four more megadroughts that severely affected Asian societies (Cook et al., 2010) are also captured in our reconstruction, along with other major droughts and pluvials. Central Asia observed a six-decade drought between 1260–1320 and sustained pluvials during 1740–1769. East Asia experienced extended drought in the second half of the fifteenth century. Most notably, Southeast Asia suffered a drought between 1225–1255 that was comparable in length to Angkor Drought I, but more severe in magnitude. Following this drought was a multi-decadal pluvial in 1271–1307. The drought is prominent in the speleothem record of Wang et al. (2019), and the pluvial can also be traced from there.

4.3 Links to Oceanic Drivers

To exemplify the spatial variation of how the oceans influence streamflow, we selected four river basins from west to east: Krishna, Chao Phraya, Mekong, and Yangtze (Figure 1), and selected one station from each basin. Because of over-year storage in the Krishna, the only station that met our data quality criteria (Section 2.1) lies in the upper reach of the river. For the other basins, we were able to choose stations in the downstream that are more representative of the basin. The names and locations of these stations are shown in Figure 3.

We calculated the correlation between reconstructed annual streamflow at each basin and the seasonal averages of global sea surface temperature (SST) for the period 1855–2012. Correlation patterns vary both seasonally and spatially, with differences among rivers and among oceans.

4.3.1 Pacific Ocean

For the Krishna, correlations are weak, and small significant correlation areas are observed in the tropical Pacific, mainly from summer to winter of the current year (Figure 6a). Tropical Pacific SST—a manifestation of the El Niño-Southern Oscillation (cf. McPhaden et al., 2006)—correlates negatively with streamflow. The hydroclimate of South Asia tends to be drier during El Niños and wetter during La Niñas. These tendencies have also been observed from tree ring records (Borgaonkar et al., 2010), reconstructed PDSI (Yu et al., 2018) and precipitation (Shi & Wang, 2018). The seasonality of correlation suggests that annual streamflow responds more strongly to an ongoing ENSO event than to a decaying one.

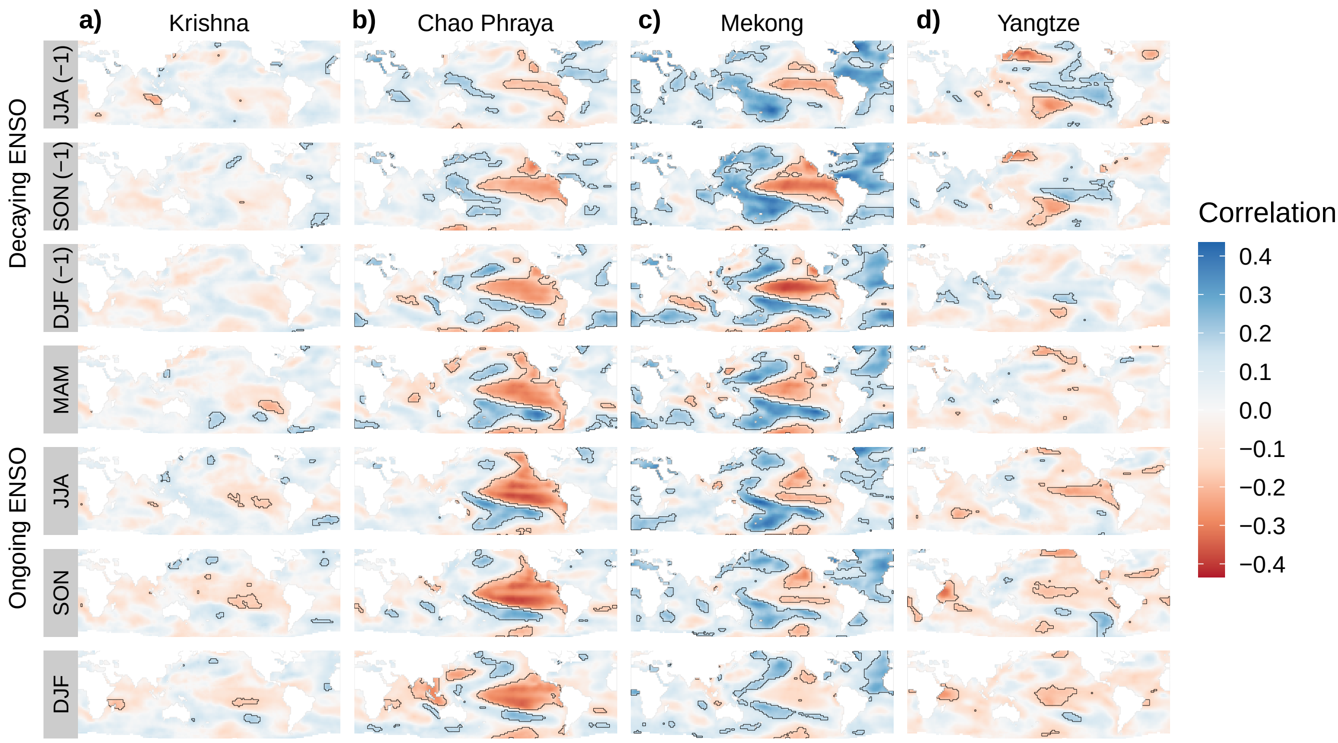

Figure 6. Correlation between reconstructed mean annual streamflow at four river basins (this work) and seasonal averages of global sea surface temperature (SST) from the NOAA_ERSST_v5 data set (Huang et al., 2017) for the period 1855–2012; significant correlations ($\alpha = 0.05$) enclosed in black boundaries. The stations used are shown in Figure 3. "(-1)" denotes previous year.

The Yangtze has a similar current summer–winter Pacific SST correlation pattern to that of the Krishna (i.e, related to ongoing ENSO events), with larger significant correlation areas. It also responds to decaying ENSO events (prior summer–winter) much more strongly than does the Krishna. Correlation with decaying ENSO events takes the opposite sign to that of ongoing ENSO events (Figure 6d). These opposite ENSO influences on eastern China have been shown in a similar seasonal correlation analysis using reconstructed precipitation (Shi & Wang, 2018) but not in the annual composite analyses of Yu et al. (2018) and Li et al. (2013). The latter two works showed wetter tendencies during El Niño and drier tendencies during La Niña, likely capturing only the decaying phase.

Unlike in the Krishna and Yangtze, streamflow in the Chao Phraya and Mekong correlates significantly with SST over most of the Pacific Ocean, and the correlation persists across all seasons, reflecting equal influences from decaying and ongoing ENSO events (Figure 6b and c). The basin-wide correlation pattern and its lack of seasonality suggest influences from a driver at longer time scales, likely the Pacific Decadal Variability (PDV)—decadal variations of Pacific SST resulted from complex tropical-extratropical ocean-atmosphere interactions (Henley, 2017). The North Pacific component of PDV is known as the Pacific Decadal Oscillation (PDO) (Mantua & Hare, 2002), its southern counterpart the South Pacific Decadal Oscillation (Shakun & Shaman, 2009); basin-wide SST variation patterns have also been termed Interdecadal Pacific Oscillation (Folland et al., 1999). These modes are closely related (Henley, 2017). The PDO has been shown to influence hydroclimatic variability in Monsoon Asia, in conjunction with ENSO (Yu et al., 2018). Specifically for the Chao Phraya, PDO also modulates ENSO's influence on peak flow (C. Xu et al., 2019). Here, by juxtaposing the correlation maps, our analyses reveal that ENSO and PDV exert their greatest influence on the Mekong and Chao Phraya.

4.3.2 Indian Ocean

We observe negative correlations between streamflow and Indian Ocean SST in current-year winter in the Chao Phraya, and to a lesser extend in the Yangtze and Krishna. These basin-wide correlation patterns follow closely after peak ENSO correlations in summer and fall, consistent with the Indo-Pacific coupling described by Saji et al. (1999): an ENSO event in the Pacific leads to SST anomalies of the same sign Indian Ocean. This mode accounts for about 30% of Indian Ocean SST variability [*ibid*]. These authors also proposed another mode—the Indian Ocean Dipole (IOD) mode, the positive phase of which is characterized by cool eastern Indian Ocean around Sumatra, and warm western Indian Ocean around East Africa. Positive IOD events often occur around June–July, peak in October and abruptly end in November, a phenomenon called seasonal locking (Saji et al., 1999; Ummenhofer et al., 2017). Positive IOD events have been linked to droughts in Southeast Asia but this relationship is not robust (Ummenhofer et al., 2013). Consistent with their results, we observe a weak east-positive–west-negative correlation pattern between Indian Ocean SST and Southeast Asia streamflow (Mekong and Chao Phraya) in the fall (the peak IOD season), both for prior- and present-year, with small areas of significant correlation. This pattern becomes stronger in prior-year winter, suggesting a lag between peak IOD and its effect to Southeast Asia, but not so for present-year winter, likely because it is dominated by the basin-wide ENSO mode (the IOD mode only accounts for 12% of Indian Ocean SST variability (Saji et al., 1999)).

4.3.3 Atlantic Ocean

The Chao Phraya and Mekong streamflow correlates positively with tropical and northern Atlantic SST. Significant and consistent correlations are observed throughout the seasons for the Mekong, but less consistent for the Chao Phraya. Wang et al. (2019) proposed a mechanism to explain relationship: increased tropical Atlantic SST leads to changes in zonal moisture transport, causing depression over tropical Indian Ocean, reducing rainout over the basin, leaving more moisture available to be transported to mainland Southeast Asia, ultimately strengthening Indian Monsoon rain over the region. This mechanism is consistent with their speleothem record and also with our streamflow reconstruction.

4.3.4 Temporal variability

Figure 6 shows how teleconnection between Monsoon Asia's streamflow and global SST varied among river basins. To see if this teleconnection also changed through time, and how, we repeated the same analysis in three sub-periods: 1855–1904, 1905–1954, and 1955–2004 (see Figure S6). We observe the following. First, our reconstruction captures the SST correlation patterns in the instrumental period (1955-2004), thereby further validating the quality of our reconstructions. Second, the SST correlation patterns changed through time for all four rivers, but more interestingly, teleconnection weakened remarkably for the Chao Phraya, Mekong, and Yangtze during 1905-1954 compared to the other two time windows.

5 Conclusions

In this work, we produce the first large-scale and long-term record of streamflow variability for Monsoon Asia, covering 48 stations in 16 countries. In making this record, we also develop a novel automated, climate-informed, and dynamic streamflow reconstruction framework that leveraged the computational advantages offered by our climate proxy—the Monsoon Asia Drought Atlas (MADA) version 2. Our framework achieves good skills for 96% of the stations, and skill distribution is spatially homogeneous. Our results provide a synoptic understanding of Monsoon Asia's streamflow variability over the past eight centuries, and reveal how the teleconnection between streamflow and its oceanic drivers varied over space and time.

From our reconstruction, streamflow in Monsoon Asia appears coherent: high and low flows often occur simultaneously at nearby stations and adjacent basins. This coherence is attributed to common oceanic drivers—the El Niño–Southern Oscillation (ENSO), the Pacific Decadal Variability (PDV), the Indian Ocean Dipole, and tropical Atlantic sea surface temperature variations. Coherence emerges even though we reconstructed each station individually, demonstrating the merits of Point-by-Point Regression. More importantly, this coherence implies that water management in Asia should be coordinated among basins. For example, Thailand is increasingly purchasing Mekong-generated hydropower from Laos, and when that is insufficient, complements its energy needs with thermal power from plants that use water from the Chao Phraya for cooling (Chowdhury et al., 2019). Thailand's energy system is at risk when a prolonged drought occurs at both rivers—our record shows such events have happened several times in the past.

We showed that the Pacific, Indian, and Atlantic Oceans contribute to streamflow variability. Therefore, water management in Monsoon Asia should take into account the ocean states. A case study of the Angat River (the Philippines) showed that reservoir operating policies informed by ENSO states are more robust than conventional policies that only account for local hydrological conditions (Libisch-Lehner et al., 2019). Operating policies may be improved further if, say, the PDV is also considered. There is probably even more potential for improving water resources management in the Mekong and Chao Phraya River Basins, as the oceanic drivers exert very strong influences on these rivers.

Acknowledgments

Hung Nguyen is supported by the President's Graduate Fellowship from the Singapore University of Technology and Design. We thank Edward Cook, Caroline Ummenhofer, Nerilie Abram, Nathalie Goodkin, Xun Sun, Murray Peel, and Rory Nathan for insightful comments. We are grateful to Thanh Dang, Mukund Rao, Rosanne D'Arrigo, Donghoon Lee, and Caroline Leland for streamflow data of the Mekong, Brahmaputra, Citarum, Han, and Yeruu Rivers. Chao Phraya River data were obtained from the Thai Royal Irrigation Department at `www.hydro1.net`, Indus River from Rao et al. (2018, Supporting Information), other streamflow data from GSIM (Do et al., 2018; Gudmundsson et al., 2018), reservoir data from GRanD v1.3 (Lehner et al., 2011), MADA v2 data from Marvel et al. (2019) at `www.dropbox.com/s/n2lo99h9qn17prg/madaV2.nc`, river network data from FLO1K (Barbarossa et al., 2018) with help postprocessing by Valerio Barbarossa, basin boundary data from HydroSHEDS (Lehner & Grill, 2013) at `hydrosheds.org`, SST data from NOAA ERSST v5 (Huang et al., 2017) provided by the NOAA/OAR/ESRL PSD, Boulder, Colorado, USA, at `www.esrl.noaa.gov/psd/`. This work was conducted with open-source software: analysis and visualization performed in R (R Core Team, 2019), maps made in QGIS, and manuscript written in LaTeX. We thank the open-source software community, especially the R package creators and maintainers, for their contribu-

tions to open science. We provide all data and code, together with a step-by-step guide to reproduce the results, in a GitHub repository (Nguyen, 2020b) available at `https://github.com/ntthung/paleo-asia`; exceptions are instrumental data of the Mekong, Yangtze, and Pearl rivers due to restrictions. Lamont contribution number XXXX.

References

Anchukaitis, K. J., Buckley, B. M., Cook, E. R., Cook, B. I., D'Arrigo, R. D., & Ammann, C. M. (2010). Influence of volcanic eruptions on the climate of the Asian monsoon region. *Geophysical Research Letters*, *37*(22), 1–5. doi: 10.1029/2010GL044843

Barbarossa, V., Huijbregts, M. A., Beusen, A. H., Beck, H. E., King, H., & Schipper, A. M. (2018, dec). FLO1K, global maps of mean, maximum and minimum annual streamflow at 1 km resolution from 1960 through 2015. *Scientific Data*, *5*(1), 180052. Retrieved from `http://www.nature.com/articles/sdata201852` doi: 10.1038/sdata.2018.52

Best, J. (2019). Anthropogenic stresses on the world's big rivers. *Nature Geoscience*, *12*(1), 7–21. Retrieved from `http://dx.doi.org/10.1038/s41561-018-0262-x` doi: 10.1038/s41561-018-0262-x

Boers, N., Goswami, B., Rheinwalt, A., Bookhagen, B., Hoskins, B., & Kurths, J. (2019, jan). Complex networks reveal global pattern of extreme-rainfall teleconnections. *Nature*. Retrieved from `http://www.nature.com/articles/s41586-018-0872-x` doi: 10.1038/s41586-018-0872-x

Borgaonkar, H. P., Sikder, A. B., Ram, S., & Pant, G. B. (2010). El Niño and related monsoon drought signals in 523-year-long ring width records of teak (Tectona grandis L.F.) trees from south India. *Palaeogeography, Palaeoclimatology, Palaeoecology*, *285*(1-2), 74–84. Retrieved from `http://dx.doi.org/10.1016/j.palaeo.2009.10.026` doi: 10.1016/j.palaeo.2009.10.026

Briffa, K. R., Jones, P. D., Pilcher, J. R., & Hughes, M. K. (1988, nov). Reconstructing Summer Temperatures in Northern Fennoscandinavia Back to A.D. 1700 Using Tree-Ring Data from Scots Pine. *Arctic and Alpine Research*, *20*(4), 385. Retrieved from `https://www.jstor.org/stable/1551336?origin=crossref` doi: 10.2307/1551336

Briffa, K. R., Jones', P. D., Schweingruber, F. H., & Osborn, T. J. (1998). Influence of volcanic eruptions on Northern Hemisphere summer temperature over the past 600 years. *Nature*, *393*(6684), 450–455. doi: 10.1038/30943

Buckley, B. M., Anchukaitis, K. J., Penny, D., Fletcher, R., Cook, E. R., Sano, M., . . . Hong, T. M. (2010, apr). Climate as a contributing factor in the demise of Angkor, Cambodia. *Proceedings of the National Academy of Sciences*, *107*(15), 6748–6752. Retrieved from http://www.pnas.org/cgi/doi/10.1073/pnas.0910827107 doi: 10.1073/pnas.0910827107

Buckley, B. M., Fletcher, R., Wang, S. Y. S., Zottoli, B., & Pottier, C. (2014). Monsoon extremes and society over the past millennium on mainland Southeast Asia. *Quaternary Science Reviews*, *95*, 1–19. Retrieved from http://dx.doi.org/10.1016/j.quascirev.2014.04.022 doi: 10.1016/j.quascirev.2014.04.022

Buckley, B. M., Palakit, K., Duangsathaporn, K., Sanguantham, P., & Prasomsin, P. (2007). Decadal scale droughts over northwestern Thailand over the past 448 years: Links to the tropical Pacific and Indian Ocean sectors. *Climate Dynamics*, *29*(1), 63–71. doi: 10.1007/s00382-007-0225-1

Chen, F., He, Q., Bakytbek, E., Yu, S., & Zhang, R. (2017, nov). Reconstruction of a long streamflow record using tree rings in the upper Kurshab River (Pamir-Alai Mountains) and its application to water resources management. *International Journal of Water Resources Development*, *33*(6), 976–986. Retrieved from https://www.tandfonline.com/doi/full/10.1080/07900627.2016.1238347 doi: 10.1080/07900627.2016.1238347

Chen, F., Shang, H., Panyushkina, I., Meko, D., Li, J., Yuan, Y., … Luo, X. (2019, aug). 500-year tree-ring reconstruction of Salween River streamflow related to the history of water supply in Southeast Asia. *Climate Dynamics*(0123456789). Retrieved from https://doi.org/10.1007/s00382-019-04948-1http://link.springer.com/10.1007/s00382-019-04948-1 doi: 10.1007/s00382-019-04948-1

Chen, F., Shang, H., Panyushkina, I. P., Meko, D. M., Yu, S., Yuan, Y., & Chen, F. (2019, may). Tree-ring reconstruction of Lhasa River streamflow reveals 472years of hydrologic change on southern Tibetan Plateau. *Journal of Hydrology*, *572*, 169–178. Retrieved from https://www.sciencedirect.com/science/article/pii/S0022169419302112 doi: 10.1016/J.JHYDROL.2019.02.054

Chen, F., Yuan, Y., Davi, N., & Zhang, T. (2016, dec). Upper Irtysh River flow since AD 1500 as reconstructed by tree rings, reveals the hydroclimatic signal of inner Asia. *Climatic Change*, *139*(3-4), 651–665. Retrieved from http://link.springer.com/10.1007/s10584-016-1814-y doi: 10.1007/s10584-016-1814-y

Chen, F., & Yuan, Y.-j. (2016, jul). Streamflow reconstruction for the Guxiang River, eastern Tien Shan (China): linkages to the surrounding rivers of Central Asia. *Environmental Earth Sciences*, *75*(13), 1049. Retrieved from http://link.springer.com/10.1007/s12665-016-5849-1 doi: 10.1007/s12665-016-5849-1

Chen, F., Yuan, Y.-j., Zhang, R.-b., Wang, H.-q., Shang, H.-m., Zhang, T.-w., . . . Fan, Z.-a. (2016, jun). Shiyang River streamflow since AD 1765, reconstructed by tree rings, contains far-reaching hydro-climatic signals over and beyond the mid-latitude Asian continent. *Hydrological Processes*, *30*(13), 2211–2222. Retrieved from http://doi.wiley.com/10.1002/hyp.10788 doi: 10.1002/hyp.10788

Chowdhury, A. F. M. K., Dang, D. T., & Galelli, S. (2019). *Impacts of Hydro-climatic Variability on the Energy System of the Greater Mekong Sub-region.* Asia Oceania Geosciences Society Annual Meeting 2019 (AOGS 2019), Singapore. Abstract number HS17-A002. Retrieved from http://www.asiaoceania.org/aogs2019/public.asp?page=browse{_}abstract.htm

Cook, E. R. (2015). *Developing MADAv2 Using The Point-By-Point Regression Climate Field Reconstruction Method.* Kyoto, Japan: 4th Asia 2k Workshop. Retrieved from http://pastglobalchanges.org/download/docs/working{_}groups/asia2k/4thAsia2k/Cook.ppsx

Cook, E. R., Anchukaitis, K. J., Buckley, B. M., D'Arrigo, R. D., Jacoby, G. C., & Wright, W. E. (2010, apr). Asian Monsoon Failure and Megadrought During the Last Millennium. *Science*, *328*(5977), 486–489. Retrieved from http://www.sciencemag.org/cgi/doi/10.1126/science.1185188http://www.ncbi.nlm.nih.gov/pubmed/20413498 doi: 10.1126/science.1185188

Cook, E. R., & Kairiukstis, L. A. (1990). *Methods of dendrochronology. Applications in the Environmental Sciences* (E. R. Cook & L. A. Kairiukstis, Eds.). Kluwer Academic Publishers.

Cook, E. R., Meko, D. M., Stahle, D. W., & Cleaveland, M. K. (1999). Drought Reconstructuions for the continental United States. *Journal of Climate*, *12*(APRIL), 1145–1162. doi: 10.1175/1520-0442(1999)012⟨1145:DRFTCU⟩2.0.CO;2

Cook, E. R., Palmer, J. G., Ahmed, M., Woodhouse, C. A., Fenwick, P., Zafar, M. U., . . . Khan, N. (2013). Five centuries of Upper Indus River flow from tree rings. *Journal of Hydrology*, *486*(August 2018), 365–375. Retrieved from http://dx.doi.org/10.1016/j.jhydrol.2013.02.004 doi: 10.1016/j.jhydrol.2013.02.004

Cook, E. R., Seager, R., Kushnir, Y., Briffa, K. R., Büntgen, U., Frank, D., . . . Zang, C. (2015). Old World megadroughts and pluvials during the Common

Era. *Science Advances*, *1*(10), 1–10. doi: 10.1126/sciadv.1500561

Dai, A., Trenberth, K. E., & Qian, T. (2004). A Global Dataset of Palmer Drought Severity Index for 18702002: Relationship with Soil Moisture and Effects of Surface Warming. *Journal of Hydrometeorology*, *5*(6), 1117–1130. doi: 10.1175/JHM-386.1

D'Arrigo, R., Abram, N. J., Ummenhofer, C., Palmer, J., & Mudelsee, M. (2011, feb). Reconstructed streamflow for Citarum River, Java, Indonesia: linkages to tropical climate dynamics. *Climate Dynamics*, *36*(3-4), 451–462. Retrieved from `http://link.springer.com/10.1007/s00382-009-0717-2` doi: 10.1007/s00382-009-0717-2

Davi, N. K., Jacoby, G. C., Curtis, A. E., & Baatarbileg, N. (2006). Extension of drought records for central Asia using tree rings: West-central Mongolia. *Journal of Climate*, *19*(1), 288–299. doi: 10.1175/JCLI3621.1

Davi, N. K., Pederson, N., Leland, C., Nachin, B., Suran, B., & Jacoby, G. C. (2013). Is eastern Mongolia drying? A long-term perspective of a multidecadal trend. *Water Resources Research*, *49*(1), 151–158. doi: 10.1029/2012WR011834

Do, H. X., Gudmundsson, L., Leonard, M., & Westra, S. (2018, apr). The Global Streamflow Indices and Metadata Archive (GSIM) Part 1: The production of a daily streamflow archive and metadata. *Earth System Science Data*, *10*(2), 765–785. Retrieved from `https://www.earth-syst-sci-data.net/10/765/2018/` doi: 10.5194/essd-10-765-2018

Folland, C. K., Parker, D. E., Colman, A. W., & Washington, R. (1999). Large Scale Modes of Ocean Surface Temperature Since the Late Nineteenth Century. In *Beyond el niño* (pp. 73–102). Berlin, Heidelberg: Springer Berlin Heidelberg. Retrieved from `http://link.springer.com/10.1007/978-3-642-58369-8{\_}4` doi: 10.1007/978-3-642-58369-8_4

Fritts, H. C. (1976). *Tree Rings and Climate*. London: Elsevier. Retrieved from `https://linkinghub.elsevier.com/retrieve/pii/B9780122684500X50010` doi: 10.1016/B978-0-12-268450-0.X5001-0

Gao, C., Robock, A., Self, S., Witter, J. B., Steffenson, J. P., Clausen, H. B., ... Ammann, C. (2006). The 1452 or 1453 A.D. Kuwae eruption signal derived from multiple ice core records: Greatest volcanic sulfate event of the past 700 years. *Journal of Geophysical Research Atmospheres*, *111*(12), 1–11. doi: 10.1029/2005JD006710

Genuer, R., Poggi, J.-m., & Tuleau-Malot, C. (2010, oct). Variable selection using random forests. *Pattern Recognition Letters*, *31*(14), 2225–2236. Retrieved from http://dx.doi.org/10.1016/j.patrec.2010.03.014https://linkinghub.elsevier.com/retrieve/pii/S0167865510000954 doi: 10.1016/j.patrec.2010.03.014

Gou, X., Chen, F., Cook, E. R., Jacoby, G., Yang, M., & Li, J. (2007). Streamflow variations of the Yellow River over the past 593 years in western China reconstructed from tree rings. *Water Resources Research*, *43*(6), 1–9. doi: 10.1029/2006WR005705

Gou, X. H., Deng, Y., Chen, F. H., Yang, M. X., Fang, K. Y., Gao, L. L., … Zhang, F. (2010). Tree ring based streamflow reconstruction for the Upper Yellow River over the past 1234 years. *Chinese Science Bulletin*, *55*(36), 4179–4186. doi: 10.1007/s11434-010-4215-z

Gudmundsson, L., Do, H. X., Leonard, M., & Westra, S. (2018, apr). The Global Streamflow Indices and Metadata Archive (GSIM) Part 2: Quality control, time-series indices and homogeneity assessment. *Earth System Science Data*, *10*(2), 787–804. Retrieved from https://www.earth-syst-sci-data-discuss.net/essd-2017-104/https://www.earth-syst-sci-data.net/10/787/2018/ doi: 10.5194/essd-10-787-2018

Gupta, H. V., Kling, H., Yilmaz, K. K., & Martinez, G. F. (2009, oct). Decomposition of the mean squared error and NSE performance criteria: Implications for improving hydrological modelling. *Journal of Hydrology*, *377*(1-2), 80–91. Retrieved from http://dx.doi.org/10.1016/j.jhydrol.2009.08.003https://linkinghub.elsevier.com/retrieve/pii/S0022169409004843 doi: 10.1016/j.jhydrol.2009.08.003

Henley, B. J. (2017). Pacific decadal climate variability: Indices, patterns and tropical-extratropical interactions. *Global and Planetary Change*, *155*(October 2016), 42–55. doi: 10.1016/j.gloplacha.2017.06.004

Hidalgo, H. G., Piechota, T. C., & Dracup, J. A. (2000, nov). Alternative principal components regression procedures for dendrohydrologic reconstructions. *Water Resources Research*, *36*(11), 3241–3249. Retrieved from http://doi.wiley.com/10.1029/2000WR900097 doi: 10.1029/2000WR900097

Hinkley, D. (1977). On Quick Choice of Power Transformation. *Applied Statistics*, *26*(1), 67. doi: 10.2307/2346869

Ho, M., Lall, U., & Cook, E. R. (2016, jul). Can a paleodrought record be used to reconstruct streamflow?: A case study for the Missouri River Basin. *Water Resources Research*, *52*(7), 5195–5212. Retrieved from http://doi.wiley.com/10.1002/2015WR018444 doi: 10.1002/2015WR018444

Ho, M., Lall, U., Sun, X., & Cook, E. R. (2017, apr). Multiscale temporal variability and regional patterns in 555 years of conterminous U.S. streamflow. *Water Resources Research*, *53*(4), 3047–3066. Retrieved from `http://doi.wiley.com/10.1002/2016WR019632` doi: 10.1002/2016WR019632

Huang, B., Thorne, P. W., Banzon, V. F., Boyer, T., Chepurin, G., Lawrimore, J. H., ... Zhang, H.-M. (2017, oct). Extended Reconstructed Sea Surface Temperature, Version 5 (ERSSTv5): Upgrades, Validations, and Intercomparisons. *Journal of Climate*, *30*(20), 8179–8205. Retrieved from `http://journals.ametsoc.org/doi/10.1175/JCLI-D-16-0836.1` doi: 10.1175/JCLI-D-16-0836.1

Knoben, W. J. M., Freer, J. E., & Woods, R. A. (2019, oct). Technical note: Inherent benchmark or not? Comparing NashSutcliffe and KlingGupta efficiency scores. *Hydrology and Earth System Sciences*, *23*(10), 4323–4331. Retrieved from `https://www.hydrol-earth-syst-sci-discuss.net/hess-2019-327/https://www.hydrol-earth-syst-sci.net/23/4323/2019/` doi: 10.5194/hess-23-4323-2019

Knoben, W. J. M., Woods, R. A., & Freer, J. E. (2018). A Quantitative Hydrological Climate Classification Evaluated with Independent Streamflow Data. *Water Resources Research*, *54*(7), 5088–5109. Retrieved from `http://doi.wiley.com/10.1029/2018WR022913` doi: 10.1029/2018WR022913

Koller, D., & Friedman, N. (2009). *Probabilistic Graphical Models: Principles and Techniques.* MIT Press. Retrieved from `https://books.google.com.sg/books?id=7dzpHCHzNQ4C`

Lavigne, F., Degeai, J. P., Komorowski, J. C., Guillet, S., Robert, V., Lahitte, P., ... De Belizal, E. (2013). Source of the great A.D. 1257 mystery eruption unveiled, Samalas volcano, Rinjani Volcanic Complex, Indonesia. *Proceedings of the National Academy of Sciences of the United States of America*, *110*(42), 16742–16747. doi: 10.1073/pnas.1307520110

Lehner, B., & Grill, G. (2013, jul). Global river hydrography and network routing: baseline data and new approaches to study the world's large river systems. *Hydrological Processes*, *27*(15), 2171–2186. Retrieved from `http://doi.wiley.com/10.1002/hyp.9740` doi: 10.1002/hyp.9740

Lehner, B., Liermann, C. R., Revenga, C., Vörösmarty, C., Fekete, B., Crouzet, P., ... Wisser, D. (2011, nov). Highresolution mapping of the world's reservoirs and dams for sustainable riverflow management. *Frontiers in Ecology and the Environment*, *9*(9), 494–502. Retrieved from `https://onlinelibrary.wiley.com/doi/abs/10.1890/100125` doi: 10.1890/100125

Li, J., Shao, X., Qin, N., & Li, Y. (2018, may). Runoff variations at the source of the Yangtze River over the past 639 years based on tree-ring data. *Climate Research*, *75*(2), 131–142. Retrieved from http://www.int-res.com/abstracts/cr/v75/n2/p131-142/ doi: 10.3354/cr01510

Li, J., Xie, S.-P., Cook, E. R., Chen, F., Shi, J., Zhang, D. D., ... Zhao, Y. (2019, jan). Deciphering Human Contributions to Yellow River Flow Reductions and Downstream Drying Using Centuries-Long Tree Ring Records. *Geophysical Research Letters*, *46*(2), 898–905. Retrieved from http://doi.wiley.com/10.1029/2018GL081090 doi: 10.1029/2018GL081090

Li, J., Xie, S.-p., Cook, E. R., Morales, M. S., Christie, D. A., Johnson, N. C., ... Fang, K. (2013, sep). El Niño modulations over the past seven centuries. *Nature Climate Change*, *3*(9), 822–826. Retrieved from http://dx.doi.org/10.1038/nclimate1936http://www.nature.com/articles/nclimate1936 doi: 10.1038/nclimate1936

Libisch-Lehner, C. P., Nguyen, H. T. T., Taormina, R., Nachtnebel, H. P., Galelli, S., LibischLehner, C. P., ... Galelli, S. (2019, apr). On the Value of ENSO State for Urban Water Supply System Operators: Opportunities, TradeOffs, and Challenges. *Water Resources Research*, *55*(4), 2856–2875. Retrieved from https://onlinelibrary.wiley.com/doi/abs/10.1029/2018WR023622 doi: 10.1029/2018WR023622

Liu, Y., Sun, J., Song, H., Cai, Q., Bao, G., & Li, X. (2010, may). Tree-ring hydrologic reconstructions for the Heihe River watershed, western China since AD 1430. *Water Research*, *44*(9), 2781–2792. Retrieved from https://www.sciencedirect.com/science/article/pii/S0043135410001272 doi: 10.1016/J.WATRES.2010.02.013

Mantua, N. J., & Hare, S. R. (2002). The Pacific Decadal Oscillation. *Journal of Oceanography*, *58*(1), 35–44. Retrieved from http://link.springer.com/10.1023/A:1015820616384 doi: 10.1023/A:1015820616384

Marvel, K., Cook, B. I., Bonfils, C. J. W., Durack, P. J., Smerdon, J. E., & Williams, A. P. (2019). Twentieth-century hydroclimate changes consistent with human influence. *Nature*, *569*(7754), 59–65. Retrieved from http://www.nature.com/articles/s41586-019-1149-8 doi: 10.1038/s41586-019-1149-8

McPhaden, M. J., Zebiak, S. E., & Glantz, M. H. (2006, dec). ENSO as an Integrating Concept in Earth Science. *Science*, *314*(5806), 1740–1745. Retrieved from http://www.sciencemag.org/cgi/doi/10.1126/science.1132588 doi: 10.1126/science.1132588

Nash, J. E., & Sutcliffe, J. V. (1970, apr). River flow forecasting through conceptual models part I A discussion of principles. *Journal of Hydrology*, *10*(3), 282–290. Retrieved from http://linkinghub.elsevier.com/retrieve/pii/0022169470902556 doi: 10.1016/0022-1694(70)90255-6

Nguyen, H. T. T. (2020a). *ldsr: Linear Dynamical System Reconstruction.* Retrieved from https://cran.r-project.org/package=ldsr

Nguyen, H. T. T. (2020b, may). *ntthung/paleo-asia.* Retrieved from https://zenodo.org/record/3818117 doi: 10.5281/ZENODO.3818117

Nguyen, H. T. T., & Galelli, S. (2018, mar). A Linear Dynamical Systems Approach to Streamflow Reconstruction Reveals History of Regime Shifts in Northern Thailand. *Water Resources Research*, *54*(3), 2057–2077. Retrieved from http://doi.wiley.com/10.1002/2017WR022114 doi: 10.1002/2017WR022114

Palmer, W. C. (1965). *Meteorological Drought. Research Paper No. 45.* U.S. Department of Commerce Weather Bureau.

Panyushkina, I. P., Meko, D. M., Macklin, M. G., Toonen, W. H. J., Mukhamdiev, N. S., Konovalov, V. G., ... Sagitov, A. O. (2018, oct). Runoff variations in Lake Balkhash Basin, Central Asia, 17792015, inferred from tree rings. *Climate Dynamics*, *51*(7-8), 3161–3177. Retrieved from http://link.springer.com/10.1007/s00382-018-4072-z doi: 10.1007/s00382-018-4072-z

Pederson, N., Hessl, A. E., Baatarbileg, N., Anchukaitis, K. J., & Di Cosmo, N. (2014). Pluvials, droughts, the Mongol Empire, and modern Mongolia. *Proceedings of the National Academy of Sciences of the United States of America*, *111*(12), 4375–4379. doi: 10.1073/pnas.1318677111

Pederson, N., Leland, C., Nachin, B., Hessl, A. E., Bell, A. R., Martin-Benito, D., ... Davi, N. K. (2013). Three centuries of shifting hydroclimatic regimes across the Mongolian Breadbasket. *Agricultural and Forest Meteorology*, *178-179*, 10–20. Retrieved from http://dx.doi.org/10.1016/j.agrformet.2012.07.003 doi: 10.1016/j.agrformet.2012.07.003

Pelletier, J. D., & Turcotte, D. L. (1997). Long-range persistence in climatological and hydrological time series: Analysis, modeling and application to drought hazard assessment. *Journal of Hydrology*, *203*(1-4), 198–208. doi: 10.1016/S0022-1694(97)00102-9

R Core Team. (2019). *R: A Language and Environment for Statistical Computing.* Vienna, Austria. Retrieved from https://www.r-project.org/

Rao, M. P., Cook, E. R., Cook, B. I., Palmer, J. G., Uriarte, M., Devineni, N., ... Wahab, M. (2018, aug). Six Centuries of Upper Indus Basin Streamflow Variability and Its Climatic Drivers. *Water Resources Research*, *54*(8), 5687–

5701. Retrieved from https://onlinelibrary.wiley.com/doi/abs/10.1029/2018WR023080 doi: 10.1029/2018WR023080

Robeson, S. M., Maxwell, J. T., & Ficklin, D. L. (2020). Bias Correction of Paleoclimatic Reconstructions: A New Look at 1,200+ Years of Upper Colorado River Flow. *Geophysical Research Letters*, *47*(1), 1–12. doi: 10.1029/2019GL086689

Saji, N. H., Goswami, B. N., Vinayachandran, P. N., & Yamagata, T. (1999, sep). A dipole mode in the tropical Indian Ocean. *Nature*, *401*(6751), 360–363. Retrieved from http://www.nature.com/articles/43854 doi: 10.1038/43854

Sano, M., Buckley, B. M., & Sweda, T. (2009). Tree-ring based hydroclimate reconstruction over northern Vietnam from Fokienia hodginsi: Eighteenth century mega-drought and tropical Pacific influence. *Climate Dynamics*, *33*(2-3), 331–340. doi: 10.1007/s00382-008-0454-y

Shakun, J. D., & Shaman, J. (2009, oct). Tropical origins of North and South Pacific decadal variability. *Geophysical Research Letters*, *36*(19), L19711. Retrieved from http://doi.wiley.com/10.1029/2009GL040313 doi: 10.1029/2009GL040313

Shi, H., & Wang, B. (2018, aug). How does the Asian summer precipitation-ENSO relationship change over the past 544 years? *Climate Dynamics*, *0*(0), 0. Retrieved from http://dx.doi.org/10.1007/s00382-018-4392-zhttp://link.springer.com/10.1007/s00382-018-4392-z doi: 10.1007/s00382-018-4392-z

Sigl, M., Winstrup, M., McConnell, J. R., Welten, K. C., Plunkett, G., Ludlow, F., ... Woodruff, T. E. (2015). Timing and climate forcing of volcanic eruptions for the past 2,500 years. *Nature*, *523*(7562), 543–549. doi: 10.1038/nature14565

Stockton, C., & Jacoby, G. C. (1976). *Long-term Surface-water Supply and Streamflow Trends in the Upper Colorado River Basin Based on Tree-ring Analyses* (Tech. Rep.). Lake Powell Research Project.

Stothers, R. B. (1984, jun). The Great Tambora Eruption in 1815 and Its Aftermath. *Science*, *224*(4654), 1191–1198. Retrieved from http://www.sciencemag.org/cgi/doi/10.1126/science.224.4654.1191 doi: 10.1126/science.224.4654.1191

Turner, S. W. D., & Galelli, S. (2016, may). Regime-shifting streamflow processes: Implications for water supply reservoir operations. *Water Resources Research*, *52*(5), 3984–4002. Retrieved from http://doi.wiley.com/10.1002/2015WR017913 doi: 10.1002/2015WR017913

Ummenhofer, C. C., Biastoch, A., & Böning, C. W. (2017). Multidecadal indian ocean variability linked to the pacific and implications for preconditioning indian ocean dipole events. *Journal of Climate*, *30*(5), 1739–1751. doi: 10.1175/JCLI-D-16-0200.1

Ummenhofer, C. C., D'Arrigo, R. D., Anchukaitis, K. J., Buckley, B. M., & Cook, E. R. (2013, mar). Links between Indo-Pacific climate variability and drought in the Monsoon Asia Drought Atlas. *Climate Dynamics*, *40*(5-6), 1319–1334. Retrieved from `http://link.springer.com/10.1007/s00382-012-1458-1` doi: 10.1007/s00382-012-1458-1

van der Schrier, G., Barichivich, J., Briffa, K. R., & Jones, P. D. (2013, may). A scPDSI-based global data set of dry and wet spells for 1901-2009. *Journal of Geophysical Research: Atmospheres*, *118*(10), 4025–4048. Retrieved from `http://doi.wiley.com/10.1002/jgrd.50355` doi: 10.1002/jgrd.50355

Wang, J. K., Johnson, K. R., Borsato, A., Amaya, D. J., Griffiths, M. L., Henderson, G. M., ... Mason, A. (2019). Hydroclimatic variability in Southeast Asia over the past two millennia. *Earth and Planetary Science Letters*, *525*, 115737. Retrieved from `https://linkinghub.elsevier.com/retrieve/pii/S0012821X19304297` doi: 10.1016/j.epsl.2019.115737

Wells, N., Goddard, S., & Hayes, M. J. (2004, jun). A Self-Calibrating Palmer Drought Severity Index. *Journal of Climate*, *17*(12), 2335–2351. Retrieved from `http://journals.ametsoc.org/doi/abs/10.1175/1520-0442{\%}282004{\%}29017{\%}3C2335{\%}3AASPDSI{\%}3E2.0.CO{\%}3B2` doi: 10.1175/1520-0442(2004)017⟨2335:ASPDSI⟩2.0.CO;2

Woodhouse, C. A., Gray, S. T., & Meko, D. M. (2006). Updated streamflow reconstructions for the Upper Colorado River Basin. *Water Resources Research*, *42*(5), 1–16. doi: 10.1029/2005WR004455

Xu, C., Buckley, B. M., Promchote, P., Wang, S. S. Y., Pumijumnong, N., An, W., ... Guo, Z. (2019). Increased Variability of Thailand's Chao Phraya River Peak Season Flow and Its Association With ENSO Variability: Evidence From Tree Ring δ 18 O. *Geophysical Research Letters*, *46*(9), 4863–4872. Retrieved from `https://onlinelibrary.wiley.com/doi/abs/10.1029/2018GL081458` doi: 10.1029/2018GL081458

Xu, J. (2015). River flow reconstruction using stalagmite oxygen isotope δ18O: An example of the Jialingjiang River, China. *Journal of Hydrology*, *529*, 559–569. Retrieved from `http://www.sciencedirect.com/science/article/pii/S0022169414010312` doi: 10.1016/j.jhydrol.2014.12.020

Yang, B., Chen, X., He, Y., Wang, J., & Lai, C. (2019). Reconstruction of annual runoff since CE 1557 using tree-ring chronologies in the upper

Lancang-Mekong River basin. *Journal of Hydrology*, *569*, 771–781. Retrieved from https://doi.org/10.1016/j.jhydrol.2018.12.034 doi: 10.1016/j.jhydrol.2018.12.034

Yang, B., Qin, C., Shi, F., & Sonechkin, D. M. (2012). Tree ring-based annual streamflow reconstruction for the Heihe River in arid northwestern China from ad 575 and its implications for water resource management. *Holocene*, *22*(7), 773–784. doi: 10.1177/0959683611430411

Yu, E., King, M. P., Sobolowski, S., Otterå, O. H., & Gao, Y. (2018, jun). Asian droughts in the last millennium: a search for robust impacts of Pacific Ocean surface temperature variabilities. *Climate Dynamics*, *50*(11-12), 4671–4689. Retrieved from http://dx.doi.org/10.1007/s00382-017-3897-1http://link.springer.com/10.1007/s00382-017-3897-1 doi: 10.1007/s00382-017-3897-1

Yuan, Y., Shao, X., Wei, W., Yu, S., Gong, Y., & Trouet, V. (2007, dec). The Potential to Reconstruct Manasi River Streamflow in the Northern Tien Shan Mountains (NW China). *Tree-Ring Research*, *63*(2), 81–93. Retrieved from http://www.bioone.org/doi/abs/10.3959/1536-1098-63.2.81 doi: 10.3959/1536-1098-63.2.81

Zhang, D., Zhang, Q., Werner, A. D., & Liu, X. (2016). GRACE-Based Hydrological Drought Evaluation of the Yangtze River Basin, China. *Journal of Hydrometeorology*, *17*(3), 811–828. Retrieved from http://journals.ametsoc.org/doi/10.1175/JHM-D-15-0084.1 doi: 10.1175/JHM-D-15-0084.1

Zhang, T., Yuan, Y., Chen, F., Yu, S., Zhang, R., Qin, L., & Jiang, S. (2018, feb). Reconstruction of hydrological changes based on tree-ring data of the Haba River, northwestern China. *Journal of Arid Land*, *10*(1), 53–67. Retrieved from http://link.springer.com/10.1007/s40333-017-0034-2 doi: 10.1007/s40333-017-0034-2